The Effects of Orientation and Crystallinity on the Solvent-Induced Crystallization of Poly(ethylene Terephthalate). I. Sorption- and Diffusion-Related Phenomena

HASAN JAMEEL, JOSHUA WALDMAN, and LUDWIG REBENFELD,
Textile Research Institute and Department of Chemical Engineering, Princeton University, Princeton, New Jersey 08540

Synopsis

This series of reports summarizes the results of an experimental research program designed to establish the effects of preexisting orientation and crystallinity on solvent-induced crystallization of poly(ethylene terephthalate) films. Dimethylformamide was used as a model for a strongly interacting solvent. Special emphasis has been given to the kinetics of crystallization and diffusion, the morphological and structural modifications, and the accompanying changes in physical properties. This article deals with solvent sorption and desorption. Solvent diffusion and the extent of crystallization decreased with increasing orientation and crystallinity in the starting films, with crystallinity being more important. Despite the semicrystalline morphology, the overall diffusion behavior was found to be Fickian, allowing the calculation of pseudodiffusion coefficients which were dependent on both the draw ratio and the treatment temperature. Solvent treatments at elevated temperatures involved a dual input of thermal and chemical energy, which caused the films to behave differently above and below the glass transition temperature. Solvent desorption and reversible swelling were also found to be dependent on preexisting structure and treatment conditions.

INTRODUCTION

The kinetics of both thermal and stress-induced crystallization have been discussed widely in the literature, while attention has only recently focused on polymers undergoing solvent-induced crystallization. It has been known for a long time that in the presence of certain interactive liquids, crystallization of amorphous polymers can take place at temperatures well below the glass transition temperature (T_g) of the polymer.[1–9] The interaction of the polymer with the solvent lowers the effective T_g of the material; and if the depression in the T_g is large enough to put the system in the crystallization temperature domain, the polymer chains will rearrange themselves into a lower free energy state.

It is self-evident that the solvent-induced crystallization process is controlled by the diffusion of the solvent into the polymer, although it will be shown here that under certain circumstances, particularly at elevated temperatures, thermal crystallization may precede and complicate the solvent process. In thermal crystallization, the entire specimen experiences an equivalent temperature for

Journal of Applied Polymer Science, Vol. 26, 1795–1811 (1981)
 CCC 0021-8995/81/061795-17$01.70

an equal period of time. On the other hand, in solvent crystallization, each planar unit of the polymer experiences a different time of crystallization, because only the polymer planes that have been penetrated by the solvent can undergo crystallization. The extent of crystallization is, therefore, proportional to the penetration distance of the solvent and to the time each planar element has been penetrated. Almost all previous measurements of solvent crystallization kinetics have shown that the increase in crystallinity is linearly dependent on time$^{1/2}$, indicating that crystallization is diffusion controlled and that the diffusion process can be described by Fick's classical differential equations.[2,3,5,7,10–12] Fickian diffusion is normally observed in the case of penetrants into polymers above T_g, while diffusion below T_g is usually non-Fickian.

Dimensional changes normally accompany the interaction between a polymer and an interactive solvent. These dimensional changes reflect both reversible swelling phenomena and irreversible changes in the fine structure and morphology of the polymer. Thermal shrinkage of thermoplastic polymers has been studied extensively.[13–16] Solvent-induced shrinkage has received increasing attention as a means of quantifying solvent–polymer interactions.[1,5,17,18]

The mechanisms for thermal and chemical (solvent-induced) shrinkage are quite similar in that polymer chain mobility is involved. When polymers are exposed to temperatures above T_g, the increased mobility allows the orientational strains existing in the polymer structure to be relieved. This manifests itself as a shrinkage, the magnitude of which is dependent on the preexisting structure. Shrinkage would be expected to increase with increasing preexisting orientation. However, in the case of a highly crystalline structure, the system is stabilized by the crystallites, and significant shrinkage is not observed at temperatures much below the melting point. In the case of solvent-induced shrinkage, the same underlying mechanism applies, except that part of the energy imparted to the system to increase polymer mobility is in the form of chemical energy arising from the polymer–solvent interaction. Expressed in another way, the effective T_g of the solvent–polymer system is significantly below the T_g of the dry polymer.

There are two complicating factors in the case of solvent-induced shrinkage. The first deals with the fact that in the case of strongly interactive systems, the T_g depression is so great that solvent-induced crystallization can take place. The second is the fact that polymer–solvent interactions, shrinkage, and solvent-induced crystallization must, by definition, take place in a highly swollen polymer matrix. As such, thermally induced and solvent-induced fine structures and morphologies are quite different. This aspect will be explored in greater detail in subsequent parts of this series.

Previous studies of solvent-induced crystallization have involved mainly unoriented amorphous polymers, although Weigmann et al.[1,17,18] and Bredereck and Koch[12] have studied the diffusion of solvents and also the subsequent solvent-induced shrinkage and crystallization of oriented semicrystalline fibers. The purpose of the work described in this paper was to establish the effects of preexisting orientation and crystallinity on the solvent-induced crystallization process. The system studied was poly(ethylene terephthalate) (PET) films using dimethylformamide (DMF) as a model strongly interacting solvent. Weigmann et al.[1] have shown that the T_g of a PET–DMF system is effectively about $-70°C$.

EXPERIMENTAL

Materials

The PET films used in this study were generously provided by G. C. Adams of E.I. du Pont de Nemours & Co., Inc. Unoriented films were drawn using two sets of rollers revolving at different speeds which determined the draw ratio. Heaters were placed between the sets of rollers—one on top of the film and one below. The heater settings determined the stretch temperature. An input power at 30% of rated heater power was used by du Pont, and this corresponds to a stretch temperature of 90–110°C. A range of draw ratios between 1.0 and 4.0 were provided. There was present both orientation and crystallinity in some of the samples resulting from the drawing as was described by Adams[22] and as is confirmed in the work being reported here.

Weight Uptake Kinetics

For weight uptake studies, samples measuring approximately 1 in. by 1/2 in. were immersed in DMF for specified lengths of time at temperatures ranging from 21 to 130°C. Upon removal, the samples were blotted twice on filter paper to remove excess solvent from the film surface. They were then placed in preweighed bottles to measure the weight uptake.

Desorption Kinetics

The desorption of DMF after immersion and removal from the solvent was investigated with a du Pont 951 thermogravimetric analyzer (TGA) coupled with a du Pont 990 thermal analyzer. This instrument measured the weight change of the material at a preselected temperature of 30°C over a period of time. All TGA runs were done under a nitrogen flow rate of 50 cc/min.

The kinetics of the dimensional changes occurring as the sample was allowed to dry after the DMF treatments were also measured. After immersion in DMF, the sample was patted between two filter papers and then dried at room temperature (21°C). The change in length was recorded as a function of time until equilibrium was reached.

Weight Loss

The TGA was also used to record the weight loss of the polymer due to the DMF treatment. Preweighed samples were placed on the TGA after solvent treatment and heated to its melting point (260°C) to drive off all entrapped volatiles. This gave the dry weight after the DMF treatment which was subtracted from the dry weight of an untreated sample measured in the same manner. The TGA was also used to determine the equilibrium weight uptake of DMF, which could then be compared to that measured from the weight uptake kinetics.

RESULTS AND DISCUSSION

Properties of Untreated Films

The density, birefringence, and dynamic modulus values of the untreated films as a function of the mechanical draw ratio are shown in Figures 1–3. The density values of the untreated samples indicate that up to a draw ratio of 2.8, there is only a small amount of crystallinity. Above this draw ratio, density increases quite rapidly, and a crystalline pattern becomes visible in the wide-angle X-ray scattering (WAXS) patterns. The degree of crystallinity calculated using an amorphous density of 1.335 g/cm^3 and a crystalline density of 1.455 g/cm^3 gives values of 1.67 and 31.1% for draw ratios of 1.6 and 4.0, respectively.

The general shape of the birefringence curve as a function of draw ratio is similar to that obtained for density, the dependence being greater at the higher draw ratios. This is in contrast to results obtained with nylon fibers by Sakuma and Rebenfeld[19] where the dependence of birefringence on draw ratio was greater at the lower draw ratios. Since crystalline regions become oriented with increasing extension to a greater extent than amorphous regions, it appears that the contribution of the crystalline birefringence to the total birefringence in these fibers is significantly greater. Therefore, the initial region of the curve in Figure

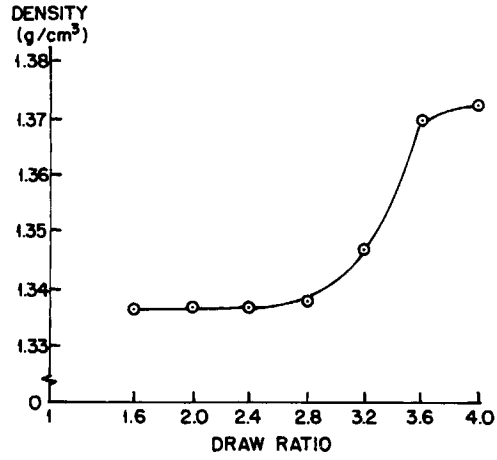

Fig. 1. Density of untreated PET films as function of draw ratio.

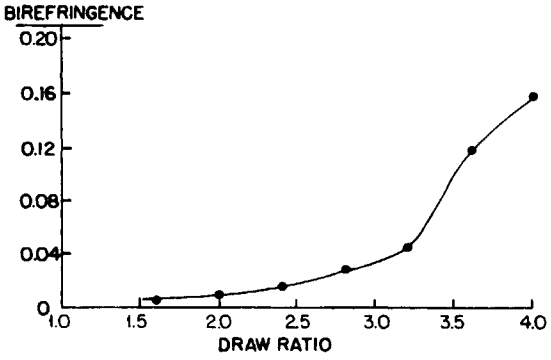

Fig. 2. Birefringence of untreated PET films as function of draw ratio. Polarizing microscope with Berek compensator method, courtesy of E. Leitz Company.

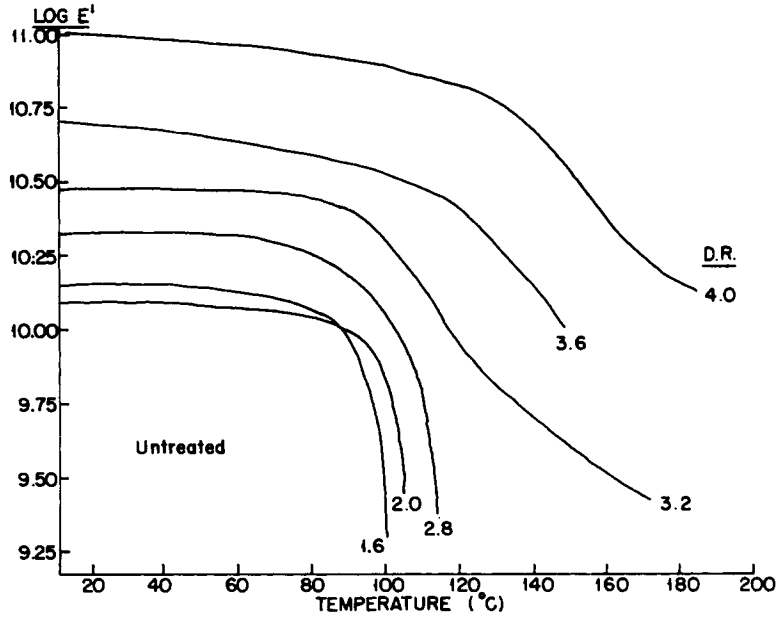

Fig. 3. Dynamic modulus E' as function of temperature for untreated PET films of various draw ratios.

2 represents the increase in birefringence due to amorphous orientation, while the sharply rising part is due to increases in both amorphous and crystalline orientations. If the birefringence curve for the amorphous films is extrapolated beyond *DR* 3.2, a rough estimate may be made of the crystalline contribution to birefringence. The birefringence curve for nylon fibers noted by Sakuma and Rebenfeld reflects principally the crystalline contribution since their nylon samples were partly crystalline even in the undrawn state. The crystalline birefringence contribution shown in Figure 2 follows a similar trend.

The dynamic modulus (E') of the highly drawn sample is about an order of magnitude greater than that of a sample with a low draw ratio (*DR* 1.6). The transition shown in Figure 3 is the α dispersion, which is related to the glass transition. A β dispersion of complex origin has also been noted in PET at about $-40°C$.[20] The estimate of the glass transition (T_g) at various draw ratios is presented in Table I. T_g increases with orientation, the shift being somewhat more prominent with the onset of crystallinity. The increase in T_g probably reflects increasing restraint of the amorphous regions by orientation and the presence of crystallites.

TABLE I
PET Film Properties

DR	Thickness, mm	T_g, °C
1.6	0.123	97
2.0	0.102	105
2.4	0.088	—
2.8	0.073	110
3.2	0.067	120
3.6	0.052	131
4.0	0.050	144

Weight Uptake Kinetics

Figures 4–7 show weight uptake data for oriented PET films of selected draw ratios at various DMF treatment temperatures. The weight uptakes are expressed in terms of the mass of liquid absorbed per weight of dry polymer and are plotted as a function of time$^{1/2}$. A pseudodiffusion coefficient can be calculated from the initial linear slope (least-squares method) of such plots after normalization for sample thickness. The thickness of the films is inversely related to the draw ratio (Table I).

The diffusion coefficients (D) as a function of the draw ratio are shown in Figure 8. The rate of liquid uptake into the films decreases with increasing draw ratio with the decrease being particularly prominent at the low draw ratios. Above a draw ratio of 3.2, the rate of uptake is very slow due to the presence of preexisting crystallinity which lowers the mobility of the amorphous chains. The

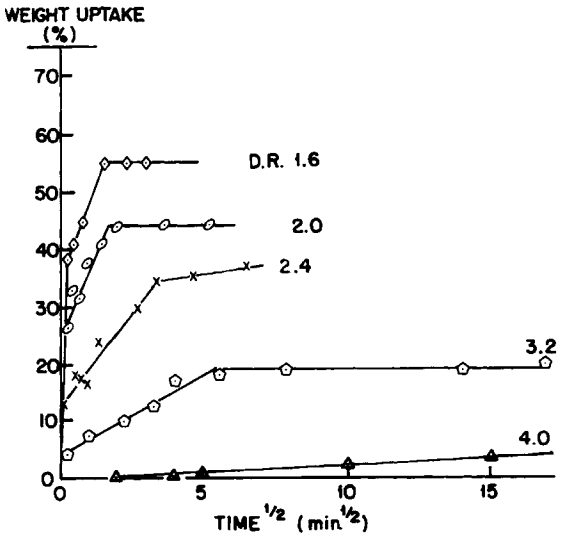

Fig. 4. Weight uptake (%) as function of the square root of immersion time in DMF at 21°C for various draw ratios.

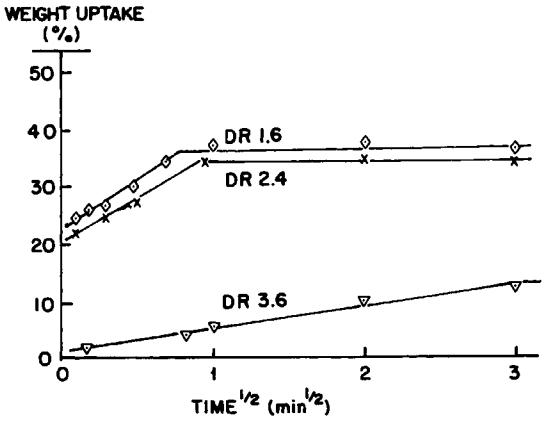

Fig. 5. Weight uptake (%) as function of the square root of immersion time in DMF at 70°C for various draw ratios.

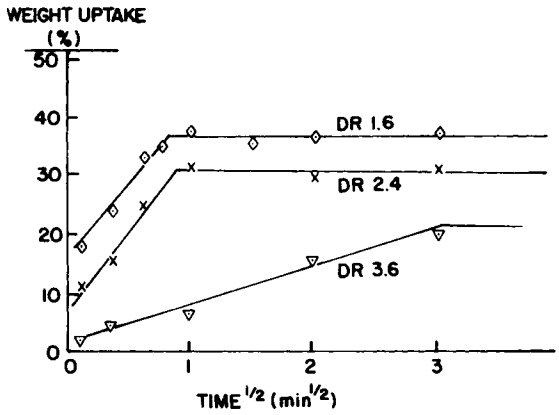

Fig. 6. Weight uptake (%) as function of the square root of immersion time in DMF at 100°C for various draw ratios.

orientation of the amorphous chains also increases the density and lowers the free volume available for the diffusion process. The diffusion coefficients are shown in Figure 9 as a function of the DMF treatment temperature for *DR* 1.6, 2.4, and 3.6 films. For the low draw-ratio sample (*DR* 1.6), only a modest temperature dependence was found up to a treatment temperature of 80°C. Above this temperature, the diffusion coefficient increased rapidly; and at 130°C, there was an order of magnitude increase in its value. The *DR* 2.4 shows similar behavior, while in the case of *DR* 3.6, a more modest increase was noticeable over the entire temperature range investigated.

The diffusion data are plotted as a function of $1/T$ in Figures 10–12 according to the Arrhenius relationship in order to provide an estimate of the activation energy (E_d) of the process. Despite the limited data, there appears to be a consistent transition in the curves for *DR* 1.6 and 2.4 at about 80°C and for *DR* 3.6 at approximately 112°C. These transitions are approximately in the range of T_g values obtained from the dynamic modulus measurements (Table I).

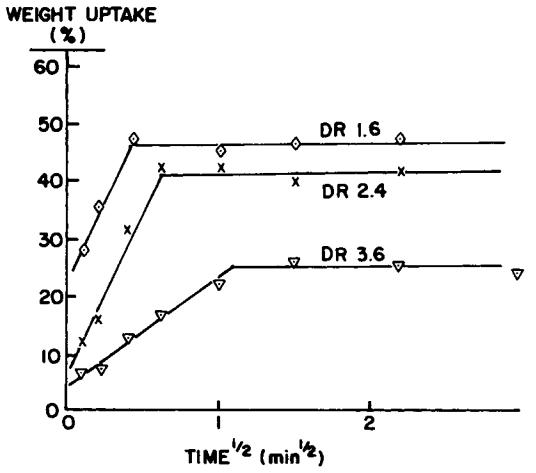

Fig. 7. Weight uptake (%) as function of the square root of immersion time in DMF at 130°C for various draw ratios.

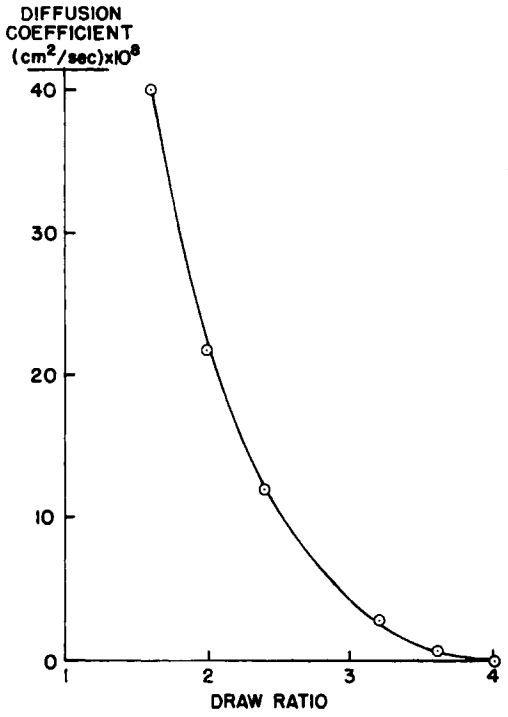

Fig. 8. Diffusion coefficient as function of draw ratio for DMF uptake at 21°C.

It is known that the solvent penetrates the polymer as a distinct diffusion front which can be observed by microscopy of fracture surfaces. Behind the front, the polymer has been completely penetrated and crystallized. Markarewicz and Wilkes[5] have mentioned that a finite gradient in solvent concentration may exist at the advancing front–dry polymer interface, but the zone where the gradient exists is probably quite narrow. In any case, the solvent has to penetrate into completely dry polymer, while the zone behind this front has been swollen and crystallized almost to equilibrium. The rate-controlling process for the diffusion will, therefore, be the penetration of the solvent into the dry polymer. Accordingly, the structure and morphology of the dry polymer will determine the rate of diffusion. Diffusion into a glassy polymer proceeds by the rigid pore mechanism, while above T_g diffusion occurs by the cooperative movement of polymer segments due to micro-Brownian motion. Diffusion in the rubbery state (above T_g) is usually more rapid than in the glassy polymer (below T_g). The DMF treatment involves both a thermal and a solvent energy input. Because of rapid heat transfer relative to mass transport, the entire bulk specimen is exposed to the treatment temperature almost instantaneously, and the PET reacts to this input of sensible heat before any significant solvent penetration has taken place. If the treatment temperature is high enough, the dry polymer will be above its T_g value, reflecting an increase in the mobility of the polymer chains.

The transition in the Arrhenius plot of the diffusion coefficient (Figs. 10–12) represents this increased segmental mobility due to the input of a sufficiently large thermal energy. The initial portion of the curve represents the diffusion

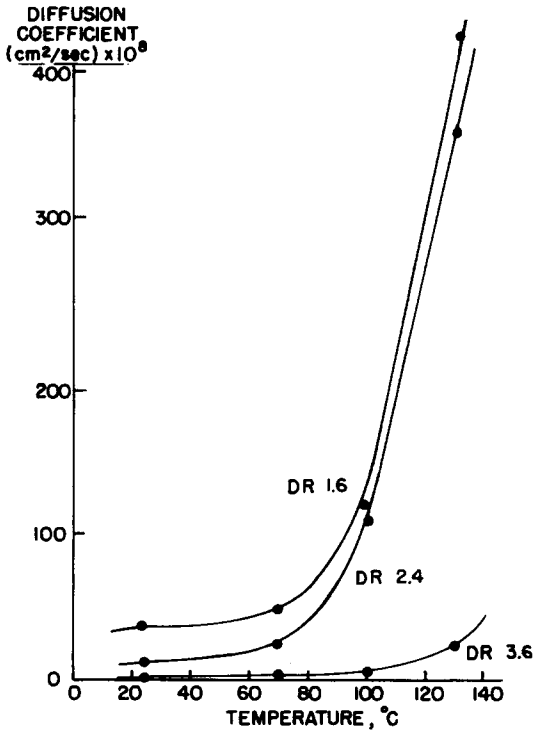

Fig. 9. Diffusion coefficient as function of DMF treatment temperature for various draw ratios.

of the solvent into a dry polymer above its glass transition temperature, while the segment with the lower slope is for diffusion into a glassy region. It should be noted that the simplified picture presented here is further complicated by the change in the crystallinity that may be occurring in the dry polymer due to the input of thermal energy. The rates of the crystallization process and the diffusion of the solvent would determine the extent to which this factor affects the overall diffusion. In a study of the rate of crystallization, Sheldon[3] noted that about 20 min was required for equilibrium at 110°C in an extruded PET film.

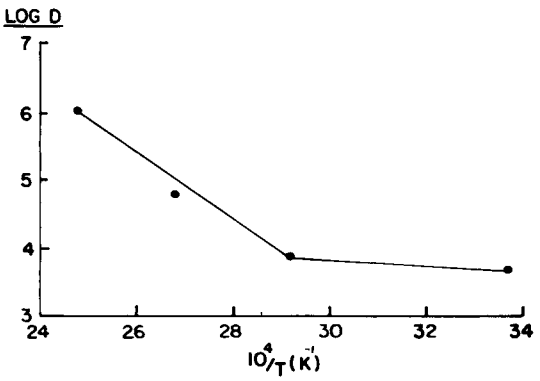

Fig. 10. Log diffusion coefficient vs. inverse of the treatment temperature for *DR* 1.6.

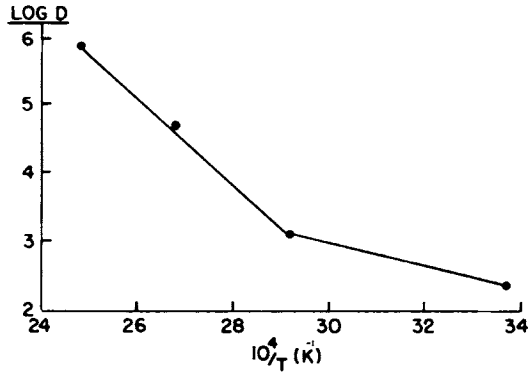

Fig. 11. Log diffusion coefficient vs. inverse of the treatment temperature for *DR* 2.4.

The activation energies (E_d), determined from the two linear regions in the Arrhenius plots, are shown in Table II. The values of E_d increase with increasing draw ratio and in the rubbery state are greater than in the glassy state. The values are somewhat lower than those found by Kashmiri and Sheldon[7] for various methyl ketones diffusing into unoriented PET films. The higher E_d in the rubbery state probably reflects the greater tortuosity of the DMF molecules as they diffuse through the PET undergoing greater segmental mobility.

Equilibrium DMF weight uptake values as a function of treatment temperature are shown in Figure 13. The equilibrium uptake reflects the relative "solubility" of the solvent in the polymer, which is dependent on the free volume and on the degree of interaction between the polymer and the liquid. In addition to the free volume, the presence of microvoids will also affect the total weight of a solvent imbibed within the polymer structure. The equilibrium weight

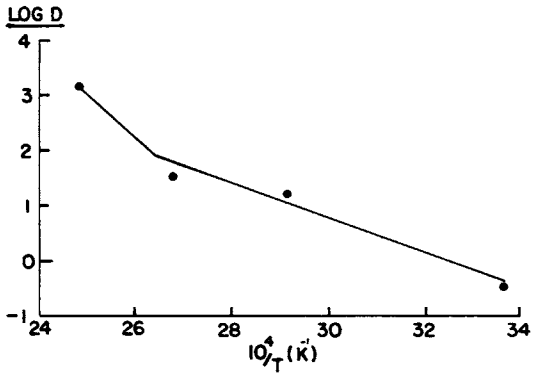

Fig. 12. Log diffusion coefficient vs. inverse of the treatment temperature for *DR* 3.6.

TABLE II
Activation Energies DMF Diffusion
(kcal/mol)

DR	Below T_g	Above T_g
1.6	0.9	9.7
2.4	3.3	12.7
3.6	6.1	15.2

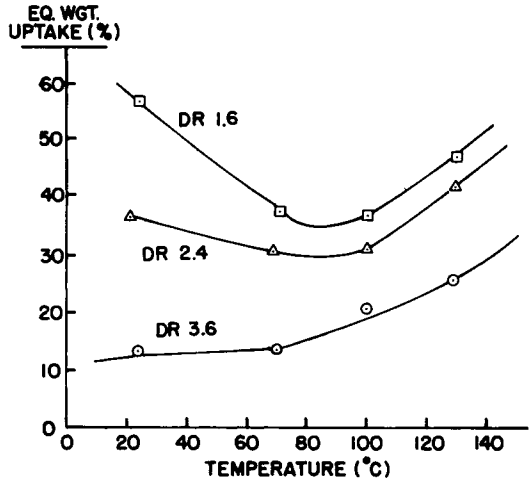

Fig. 13. Equilibrium weight uptake as function of the DMF treatment temperature for various draw ratios.

uptake goes through a minimum for draw ratios 1.6 and 2.4. With increasing treatment temperature the degree of crystallinity is increased which would decrease the free volume present. However, increasing severity of treatment also results in the creation of microvoids due to rapid crystallization in a swollen state. Both these factors affect the equilibrium uptake, one decreasing and the other increasing the quantity of solvent that can be held. The net result is the appearance of a minimum at about 90°C. At draw ratio 3.6, the DMF causes little change in crystallinity until a treatment temperature of 100°C is reached. At that temperature, there is again an increase in both crystallinity and void volume, with the effect of the voids being predominant. Weigmann[21] has shown that voids in PET fibers occur after a DMF treatment of 100°C with a subsequent increase in the relative dye uptake. Kashmiri and Sheldon[7] in their work with amorphous PET and ketones reported that the equilibrium uptake was independent of temperature. The temperatures used in their study ranged from 25 to 45°C, a range which was apparently not broad enough to observe some of the effects discussed above.

It is also of interest to note that the linear portions of the weight uptake curves (Figs. 4–7) do not all pass through the origin when extrapolated to zero time. This very rapid weight uptake at short times has also been noted by Desai and Wilkes[2] and by Makarewicz and Wilkes[5] and may be attributed to surface cavitation. The cavitation exposes a high surface area to the liquid, and a significant volume of the solvent is entrapped within the cavitated surface region. The cavitated surface structure develops almost instantaneously upon immersion into a highly interactive solvent and will be discussed in greater detail in part II of this series. Some other pertinent data from the weight uptake measurements are summarized in Table III.

Desorption and Reversible Swelling

In addition to DMF uptake of the untreated films, desorption of the DMF during drying from the solvent-treated film was also measured by means of thermogravimetry. Figures 14 and 15 show desorption values as a function of

TABLE III
Results from DMF Weight Uptake Measurements

Temp., °C	Time at equilibrium, min	Equilibrium sorption, %	D, cm²/s
	DR 1.6 (Film Thickness = 0.123 mm)		
21	0.72	56.6	40×10^{-8}
70	0.64	35.0	49×10^{-8}
100	0.64	36.0	120×10^{-8}
130	0.16	46.0	410×10^{-8}
	DR 2.4 (Film Thickness = 0.088 mm)		
21	3.8	35.0	11×10^{-8}
70	0.81	30.0	23×10^{-8}
100	0.81	31.0	110×10^{-8}
130	0.36	41.0	360×10^{-8}
	DR 3.6 (Film Thickness = 0.052 mm)		
21	64.0	13.5	0.65×10^{-8}
70	9.0	12.5	3.5×10^{-8}
100	9.61	21.0	4.7×10^{-8}
130	1.21	25.0	24.0×10^{-8}

the square root of drying time. The linear portions of these curves do not always pass through the initial point at time zero, in which case this experimental point has a lower value. This deviation of the initial data point from the linear region is most pronounced at the low draw ratios. The initial desorption rate is affected to a large degree by the surface morphology which is cavitated at the low draw ratios. With decreasing surface cavitation (increasing *DR*), the initial point tends to lie on the straight line. The surface cavitation introduces a discontinuity in the desorption behavior, as was previously noted in the weight uptake kinetics.

The linearity of the desorption data as a function of time$^{1/2}$ implies apparent Fickian diffusion. Most of the solvent absorbed is held either within the amorphous regions or within the microvoids created by solvent crystallization. As crystallization proceeds in the polymer, the solvent is excluded from devel-

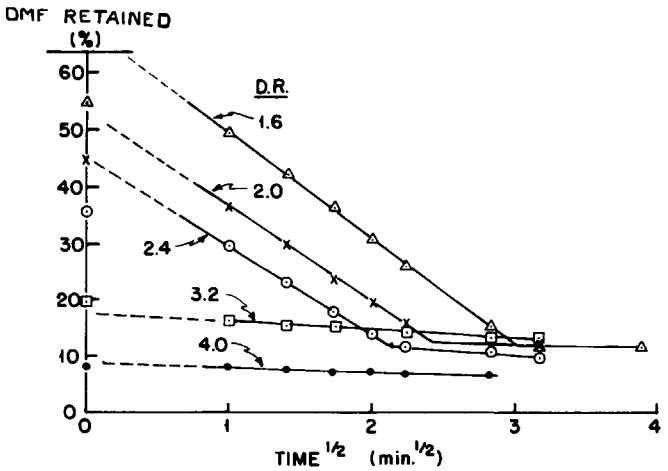

Fig. 14. Desorption of DMF at 30°C expressed as wt % of DMF absorbed as function of the square root of the desorption time. The samples were initially treated in DMF at 21°C for 1 h.

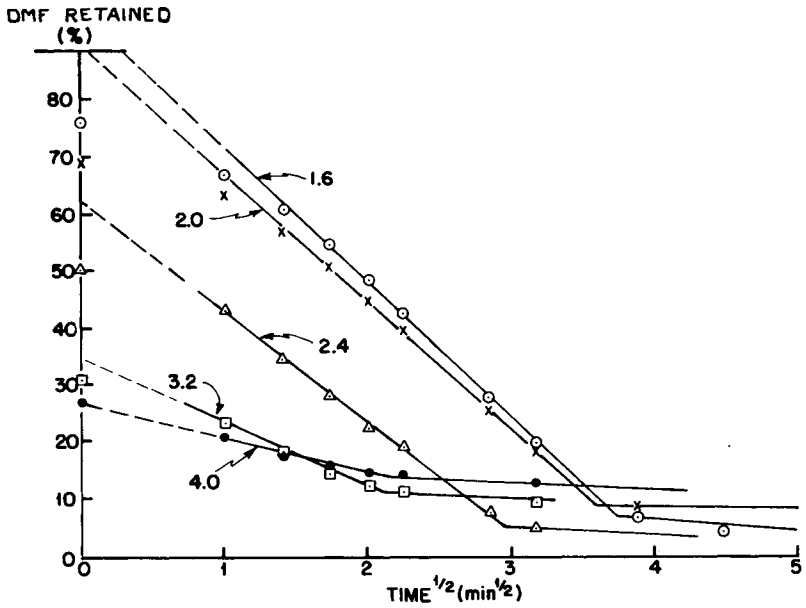

Fig. 15. Desorption of DMF at 30°C expressed as wt % of DMF absorbed as function of the square root of the desorption time. The samples were initially treated in DMF at 145°C for 10 min.

oping crystallites into the amorphous regions. In a desorption experiment, the concentration in the film is more uniform and there is no phase change involved, so the effects of internal stresses will be smaller than during absorption. The morphologic changes that occur during absorption are irreversible, but little change occurs during the desorption process.

Most of the solvent entrapped in the structure is desorbed rather rapidly (5–10 min) under the conditions of the desorption experiment. About 10–15% weight of DMF appears to be entrapped but actually is desorbed at a significantly slower rate. The data presented in Figures 14 and 15 do not show the slow desorption process, although it would be evident if the data were plotted to a longer time scale. Apparently, a certain fraction of the DMF is held more loosely in the semicrystalline PET structure. In cases where the effect of DMF on the structure is small (DMF 21°C, *DR* 3.2 and 4.0) there is no rapid desorption, and most of the DMF is desorbed in the slow mode.

Eichhoff and Zachmann,[23] using NMR, showed that trace amounts of acetone penetrate and are held within the crystalline structure when PET is exposed to the solvent for long periods of time. Hughes and Sheldon,[24] in support of the above, noted that very small amounts of acetone were trapped in PET up to the melting point of the polymer. In addition to solvent entrapment within PET crystallites, solvent removal is made difficult by the fact that as more liquid desorbs from the film, the polymer becomes increasingly glassy.

The deswelling (shrinkage) and the structural changes that take place during DMF desorption were also studied. The shrinkage kinetics are plotted in Figures 16–19 where shrinkage is measured both in the longitudinal (draw) and transverse directions. Transverse shrinkage is defined as the dimensional change in a direction perpendicular to the draw direction. Both the longitudinal and transverse shrinkages are reversible upon reimmersion in DMF, confirming that

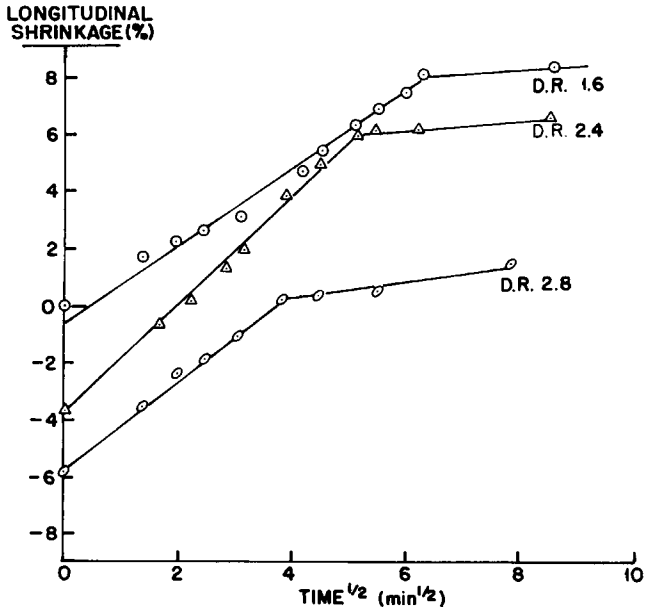

Fig. 16. Longitudinal shrinkage (deswelling) as function of the square root of the drying time at 21°C after DMF treatment at 21°C for 1 h.

these dimensional changes accompanying desorption are deswelling phenomena. The linearity of the plot of shrinkage as a function of the square root of time suggests that shrinkage is controlled by DMF desorption from the film. The time scale of desorption and that of shrinkage are of the same order, although the weight loss measurements were done under slightly different conditions.

Both the longitudinal and transverse shrinkages as a function of drying time reflect desorption and deswelling of the films after the DMF treatment. The considerable longitudinal shrinkage as a function of drying time after treatment

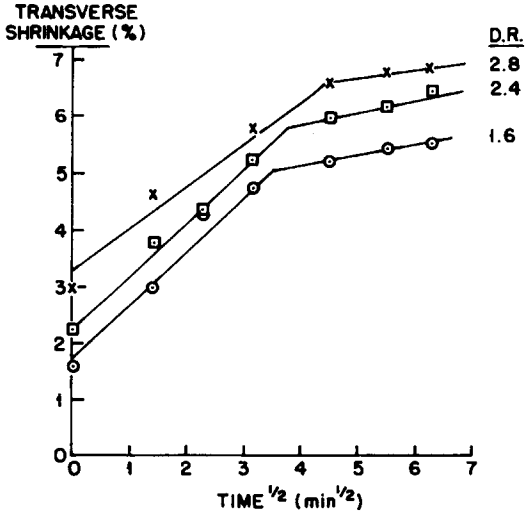

Fig. 17. Transverse shrinkage (deswelling) as function of the square root of the drying time at 21°C after DMF treatment at 21°C for 1 h.

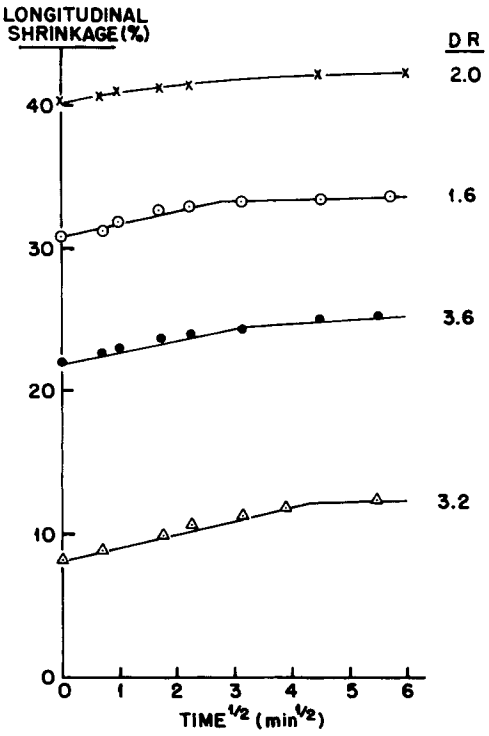

Fig. 18. Longitudinal shrinkage (deswelling) as function of the square root of the drying time at 21°C after DMF treatment at 145°C for 10 min.

with DMF at 21°C (Fig. 16) indicates a high level of swelling, although the dimensional change caused by the DMF treatment is relatively minor (zero time points). As expected, the reversible longitudinal swelling decreases with increasing orientation (draw ratio). In the case of transverse shrinkage (Fig. 17), swelling increases with increasing axial orientation (draw ratio).

The longitudinal shrinkage as a function of drying time after DMF treatment at 145°C (Fig. 18) is quite minor, indicating the stabilized structure after the high-temperature DMF treatment. The structural change and stabilization are also evident from the high shrinkages after DMF treatment before drying (zero time points). On the other hand, in contrast to longitudinal changes, there is considerable transverse deswelling upon drying (Fig. 19).

Weight Loss

The losses in weight that resulted from DMF treatments at 21°C and 145°C are shown in Table IV. The weight loss may be attributed to the extraction of oligomers and of low molecular weight material. Blackadder[25] also noted a loss of material in permeation studies using solvating liquids. The soluble fraction consisted largely of low-molecular-weight polymer as determined by viscosity. The amount of material lost is dependent on both the treatment temperature and the draw ratio. At low draw ratios, the solvents interact more extensively with the polymer, forming a more porous and surface-cavitated structure. It should be noted, however, that at *DR* 1.6 with a 21°C DMF treatment, a cavitated

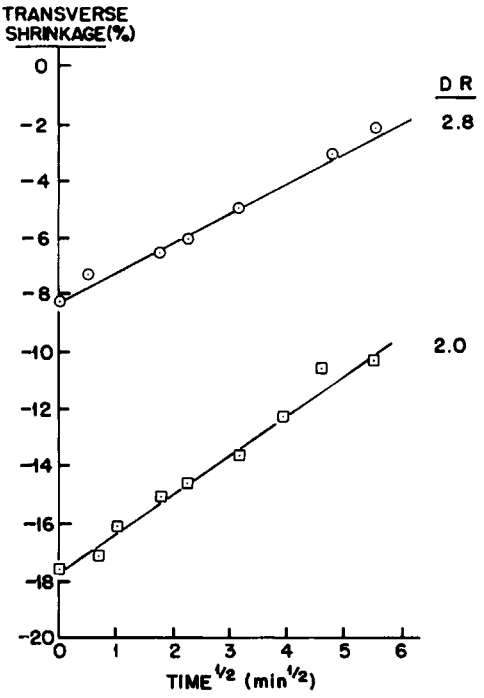

Fig. 19. Transverse shrinkage (deswelling) as function of the square root of the drying time at 21°C after DMF treatment at 145°C for 10 min.

surface is visible (subsequent parts of this series), even though there is a loss of only 0.90% by weight, proving that surface cavitation is not associated with etching or extraction. The high-temperature solvent crystallization results in the extraction of a significant fraction of the polymer.

Conclusions

DMF sorption by PET films, as well as desorption, follows Fickian diffusion behavior. Although diffusion coefficients increase with increasing temperature, apparent activation energies are greater above T_g. The effects of increasing orientation (draw ratio) are to decrease the diffusion coefficient and to increase the activation energy. The kinetic aspects of DMF diffusion into PET as well as the equilibrium DMF uptake are complicated by both solvent and thermal crystallization processes.

TABLE IV
Weight Losses (%) on DMF Treatment

DR	DMF (at 21°C)	DMF (at 145°C)
1.6	0.90	8.75
2.0	0.62	7.91
2.4	0.47	4.12
3.6	—	0.40
4.0	0.05	0.22

The authors are pleased to acknowledge many helpful discussions with Dr. H.-D. Weigmann of TRI. The work was made possible by grants from the National Science Foundation (Grant No. 76-80570) and from The Camille and Henry Dreyfus Foundation.

References

1. H.-D. Weigmann, A. S. Ribnick, and L. Rebenfeld, *Text. Res. J.*, **43,** 176 (1973).
2. A. B. Desai and G. L. Wilkes, *J. Polym. Sci. Symp. No.*, **46,** 291 (1974).
3. R. P. Sheldon, *Polymer*, **3,** 27, (1962).
4. H. J. Kolb and E. F. Izard, *J. Appl. Phys.*, **20,** 571 (1949).
5. P. J. Makarewicz and G. L. Wilkes, *J. Polym. Sci.*, **16,** 1529 (1978).
6. P. J. Makarewicz and G. L. Wilkes, *J. Polym. Sci.*, **16,** 1559 (1978).
7. M. I. Kashmiri and R. P. Sheldon, *Br. Polym. J.*, **1,** 65 (1969).
8. W. R. Moore and R. D. Sheldon, *Polymer*, **2,** 315 (1961).
9. L. Mandelkern, *J. Appl. Phys.*, **26,** 443 (1955).
10. J. Boon and J. M. Azcue, *J. Polym. Sci.*, **6,** 885 (1968).
11. H. G. Zachmann and G. Konrad, *Makromol. Chem.*, **118,** 189 (1968).
12. K. Bredereck and E. Koch, *Melliand Textilb.*, **55,** 157 (1974).
13. M. P, Wilson, *Polymer*, **15,** 277 (1974).
14. J. H. Dumbleton, *Polymer*, **10,** 539 (1969).
15. G. M. Bhatt and J. P. Bell, *J. Polym. Sci.*, **14,** 575 (1976).
16. A. S. Ribnick, *Text. Res. J.*, **39,** 428 (1969) and **39,** 742 (1969).
17. B. H. Knox, H.-D. Weigmann, and M. G. Scott, *Text. Res. J.*, **45,** 203 (1975).
18. A. S. Ribnick and H.-D. Weigmann, *Text. Res. J.*, **43,** 316 (1973).
19. Y. Sakuma and L. Rebenfeld, *J. Appl. Polum. Sci.*, **10,** 637 (1966).
20. K. H. Illers and H. Breuer, *J. Colloid Sci.*, **18,** 1 (1963).
21. H.-D. Weigmann, M. G. Scott, A. S. Ribnick, and L. Rebenfeld, *Text. Res. J.*, **48,** 574 (1978).
22. G. C. Adams, *Polym. Prep., Am. Chem. Soc. Div. Polym. Eng. Sci.*, **19,** 456 (1979).
23. V. Eichhoff and H. G. Zachmann, *Makromol. Chem.*, **147,** 4 (1971).
24. M. A. Hughes and R. P. Sheldon, *J. Appl. Polym. Sci.*, **8,** 1541 (1964).
25. D. A. Blackadder and J. S. Keniry, *J. Appl. Polym. Sci.*, **17,** 351 (1973).

Received September 26, 1980
Accepted December 17, 1980